Hindawi
International Journal of Energy Research
Volume 2024, Article ID 2119169, 19 pages
https://doi.org/10.1155/2024/2119169

WILEY | Hindawi

Research Article

A Novel Designation of Solid Oxide Fuel Cell-Integrated System Using LPG as Fuel for Marine Vessels

Phan Anh Duong,[1] **Bo Rim Ryu**,[1] **Jinwon Jung**,[2] **Sangmok Lee**,[3] **Kyoung-Kuk Yoon**,[4] **and Hokeun Kang**[5]

[1]*Department of Marine System Engineering, Korea Maritime and Ocean University, Busan, Republic of Korea*
[2]*Fuel Gas Technology Center, Korea Marine Equipment Research Institute, Busan, Republic of Korea*
[3]*Shipbuilding and Ocean Equipment Industry Empowerment Center, Kunsan National University, Gunsan, Republic of Korea*
[4]*Division of Maritime AI & Cyber Security, Korea Maritime and Ocean University, Busan, Republic of Korea*
[5]*Division of Coast Guard Studies, Korea Maritime and Ocean University, Busan, Republic of Korea*

Correspondence should be addressed to Kyoung-Kuk Yoon; kkyoon@kmou.ac.kr and Hokeun Kang; hkkang@kmou.ac.kr

Received 26 September 2023; Revised 17 February 2024; Accepted 9 March 2024; Published 30 April 2024

Academic Editor: Arun Thirumurugan

This research showcases the seamless integration of solid oxide fuel cells (SOFC) with waste heat recovery systems, utilizing liquefied petroleum gas (LPG) as the primary fuel source. The focus of the study is on efficiently harnessing the cold energy from the LPG supply to produce substantial power for the entire system. To optimize energy utilization, a gas turbine (GT) and steam Rankine cycle (SRC) are integrated to effectively convert waste heat from the system into useful work and power. Additionally, a waste heat boiler (WHB) is incorporated to provide superheated vapor steam for seafarer accommodation. A detailed thermodynamic analysis and investigation of the proposed integrated system are performed. The simulations and optimizations of combined system are conducted using ASPEN HYSYS V12.1. Thermodynamic equations based on the fundamental laws of thermodynamics are employed to estimate system performance indicators, and the exergy destruction in major components is assessed to optimize the system's design and operation. The proposed system exhibits impressive energy and exergy efficiencies, calculated at 52.65% and 51.10%, respectively. Moreover, the waste heat recovery combined cycles contribute an additional 1,759.73 kW, equivalent to 31.65% of the total system output. The innovative models are validated against experimental data from the literature, demonstrating strong agreement. Furthermore, a comprehensive parametric study investigates the influence of varying the current density from 900 to 1,950 A/m^2, leading to a total energy efficiency variation of 41.59%, ranging from 82.45% to 40.86%. The organic Rankine cycle (ORC) performs exceptionally well, capitalizing on both cold energy and high-temperature waste heat to achieve high energy recovery efficiency. The WHB is capable of providing 8,200 kg/h of superheated vapor stream at 151°C and 499 kPa for seafarer accommodation and heating purposes. The economic viability analysis is conducted to assess the potential for investment, maintenance costs, and the payback period associated with the proposed system.

1. Introduction

Maritime transportation significantly contributes to global greenhouse gas (GHGs), nitrogen oxide (NO_x), and sulfur oxide (SO_x) emissions [1]. It is estimated that shipping activities account for approximately 3-5% of total worldwide carbon dioxide (CO_2) and about 5% of sulfur oxide (SO_x) emissions [2]. In response to growing environmental issues, the International Maritime Organization (IMO) and local maritime governing bodies have implemented strict regulations and standards for emission control [3]. Notably, initiatives like IMO 2020, MARPOL 73/78, and IMO tiers I, II, and III have been introduced. As a result, the marine sector is currently transitioning towards cleaner and more

sustainable energy alternatives. In this context, various alternative fuels are gaining prominence, including liquified petroleum gas (LPG), ethanol, compressed natural gas (CNG), biodiesel, liquified natural gas (LNG), and hydrogen. Among these alternatives, LPG stands out due to its capacity for reducing carbon emissions and providing superior fuel efficiency when compared to conventional fuels like gasoline and diesel [4]. One of the benefits of LPG is its ability to easily liquefy at room temperature and pressure of 2 kg/cm^2 or higher. This characteristic enables convenient transport and storage as it significantly reduces the volume of the gas during the liquefaction process [5].

Liquefied petroleum gas (LPG) is a liquid mixture primarily composed of propane and butane. Propane, normally gaseous under standard conditions, can transform into a liquid state when subjected to moderate pressure (8.4 bar at 20°C). On the other hand, butane comes in two forms: n-butane and iso-butane, each with boiling points of -0.5°C and -12°C, respectively. Both isomers have higher boiling points than propane, making them easier to liquefy under lower pressure. For onshore storage, propane tanks are equipped with safety valves to maintain pressure below 25 bar. Due to the lower density of LPG, its fuel tanks are larger compared to oil tanks. There are two storage options for LPG: under pressure or refrigerated. Pressurized LPG fuel tanks are preferred for their simplicity and flexibility. Vessels can conveniently bunker using pressurized tanks or semirefrigerated tanks without significant modifications. In terms of environmental impact, LPG combustion results in about 16% fewer CO_2 emissions compared to heavy fuel oil (HFO). This makes LPG a more environmentally friendly alternative [6]. When considering the entire life cycle, including fuel production, the overall CO_2 savings are approximately 17%.

In the maritime sector, LPG serves as a primary fuel source for various applications, including fuel cells, internal combustion engines (ICE) [7], or gas turbines (GT) [8]. However, using ICE presents challenges related to space requirements, maintenance efforts, and significant noise generation. Conversely, fuel cells offer a more promising solution for marine use due to their quieter operation (without moving parts) and reduced reliance on auxiliary systems. Among fuel cell types, solid oxide fuel cells (SOFC) [9, 10] prove particularly advantageous for ships. It not only reduces emission pollution and noise but also provides the flexibility to comply with environmental regulations, making them the most commercially viable option for the maritime industry [11, 12]. SOFC, as a high-temperature fuel cell, demonstrates the capability to generate substantial high-potential exhaust heat, which contributes to its enhanced energy efficiency [13, 14]. It efficiently converts chemical energy into electricity and can accommodate different types of fuel for its operation [15, 16]. LPG has emerged as an exceptionally promising fuel option for fuel cells, primarily attributed to its cost-effectiveness, ease of storage and transportation, lower flammability compared to alternative fuels, and its inherent safety features, including a detectable odor in case of leakage. Unlike other fuels such as ammonia, the utilization of LPG as a fuel in SOFCs results in thermal cracking at the anode, generating hydrogen without the necessity for steam, thereby mitigating the formation of nitrogen oxide (NO_x). Moreover, the well-established infrastructure of LPG technology contributes to a burgeoning interest in the utilization of LPG-fed fuel cells, particularly in the context of SOFCs. This interest is fueled by the combination of LPG's unique advantages and the established technology landscape, making it an increasingly attractive choice for powering SOFCs. Furthermore, the regasification process of LPG can be seamlessly integrated with power production cycles. The cold energy produced during this regasification process, at varying temperatures, can be effectively utilized to provide cooling capacity. This LPG cold energy has found successful applications in various sectors, including refrigeration and air conditioning systems, food storage, seawater desalination, air separation systems, and power generation.

Bessekon et al. [17] introduced a concept for a vehicle powered by SOFC technology in conjunction with a battery system, utilizing CNG, LNG, or LPG as potential fuels. They developed a model that integrates an SOFC into a modified Nissan Leaf Acenta electric vehicle, taking standardized driving cycles into account. The simulation involved a 30 L fuel tank and a 12 kW SOFC module, incorporating a partial oxidation fuel reformer. The results indicate a notable increase in the driving range when combining the battery-powered vehicle with an SOFC. Among the various fuels considered, LPG demonstrates competitive performance in comparison to petrol and diesel. Chen et al. [18] developed a catalyst for the prereforming of propane at an approximately 0.5 ratio of steam to carbon (S/C). They combined this prereforming process with the direct utilization of the resulting reformate in low-temperature solid oxide fuel cells (SOFCs). During the prereforming stage, propane was converted into smaller molecules, including CH_4, CO, CO_2, and H_2. The researchers observed 247 mW/cm^2 of peak power density when they directly supplied the prereformed propane to an SOFC operating at 600°C. Remarkably, even after a continuous working for 10 hours at 600°C, there was no carbon deposition observed in the fuel cell. These findings suggest that prereforming has the potential to significantly increase the working performance of low-temperature SOFCs that utilize higher hydrocarbon fuels. Ahmed et al. [19] experimented LPG supplying to the 5 kW SOFC systems with six different commercial catalysts. The catalyst's activity remained stable throughout the observation period, with no signs of degradation. Throughout the long-term test, the LPG reformer consistently produced a methane-rich mixture, containing 25% H_2, 55% CH_4, and 20% CO_2. A demonstration was conducted on a 5 kW class SOFC system, powered by commercially available LPG. The system operated using a 2×2 array stack comprising 160 cells, generating an output of over 1 kW. Emordi et al. [20] performed the thermodynamic analysis with SOFC system fueled by butane, methanol, and propane. The findings revealed that the butane configuration exhibited the highest energy efficiency at 50.3%. On the other hand, the methanol and propane systems had energy efficiencies of 46.5% and 47.7%, respectively. In terms of total energy production, the methanol fuel system generated 273.66 kW, the propane fuel system produced 234.67 kW, and the butane fuel system

generated 263.92 kW. Liu et al. [21] analyzed the performance of n-type $F_eB_bO_4$ anode of SOFC with LPG as fuel under 700°C of operating temperature. During operation, a full cell utilizing $Ti_{0.36}(Fe_{0.985}Nb_{1.015})_{0.84}O_4$ as the anode exhibits a 180 mW.cm^{-2} of power density at 700°C when exposed to 5% H_2. To enhance the electrocatalytic properties, 0.5 wt% P_d is impregnated into the cell. The main source of electric loss in this proposed configuration is attributed to the electrolyte. However, over time, the oxide anode undergoes a degradation of 20% during 5 to 26 hours of aging. Despite this, the occurrence of carbon deposition is minimal after a 5-hour operation using LPG fuel. Yan et al. [22] proposed an SOFC-integrated system employing LPG, natural gas, biogas, and water gas as fuel. This paper clearly demonstrates the efficiency and cost-effectiveness of the proposed hybrid SOFC-PEMFC system for power generation. The payback period for the investment is approximately 0.8 to 1.2 years, and the annual return on investment is calculated to be about 11 to 12%. Antolini [23] conducted an examination of the characteristics of direct propane fuel cells for energy generation, evaluating their performance in comparison to fuel cells fueled by hydrogen and methane. Propane stands out as an exceptionally suitable fuel for diverse applications, including portable devices, individual equipment, and miniaturized power supply for aerospace applications, such as fuel cells. Its advantage lies in its ease of compression, storage, and transportation, particularly as a liquid at a pressure of approximately 10 bars, distinguishing it from methane or natural gas. Additionally, the energy density of liquid propane surpasses that of methanol. The article delves into the primary challenges associated with direct propane conversion in SOFCs, including catalyst deactivation due to carbon deposition on the anode, sulfur poisoning (especially for nickel-based catalysts), and the chemical and physical compatibility of the electrolyte with anode and cathode catalysts. The discussion extends to the ongoing efforts in developing new catalysts to address these challenges.

Based on the existing literature, the integration of LPG cold energy and waste heat recovery within the system can lead to notable enhancements in both output power and thermal efficiency. However, the extent of these gains relies on the appropriateness of the chosen bottoming cycle. A successful system design is contingent upon the careful selection of suitable integrating and bottoming cycles. Hence, to optimize overall system performance, it is imperative to consider both waste heat recovery cycles and the utilization of cold energy [24]. The main target of this research is to establish a combined system that integrates LPG and SOFC technology to effectively reduce greenhouse gas emissions and adhere to IMO emission standards. The proposed approach entails incorporating an ORC with LPG as a heat sink to recover cold energy from LPG. Additionally, the study proposes the integration of SRC system with a WHB to capture and utilize high-temperature exhaust heat from SOFCs. Hence, the novelty of this work lies in the following:

(i) Proposing an innovative system integrating an ORC, SOFC, GT, SRC, and WHB designed for retrofitting into existing marine vessels

(ii) The newly devised system undergoes a comprehensive study employing three distinct approaches:

  (a) Conducting energy analysis to scrutinize the overall efficiency of the proposed system and the waste heat recovery subsystem

  (b) Employing process modeling through ASPEN HYSYS to elucidate the functionality of the proposed system, optimizing data-driven visual representation

  (c) Performing exergy analysis to explore the exergy destructions of individual system components and entire system

(iii) Conducting an extensive parametric study to analyze the system's response to variations in key indicators and parameters, aiming to identify optimal operating conditions and configurations

(iv) Undertaking an economic analysis to provide a comprehensive overview of the feasibility and applicability of the system in real-life scenarios

The specific research objectives are outlined as follows:

(i) To propose and investigate the use of LPG SOFC as an environmentally friendly solution for marine vessels, aiming to reduce emissions and comply with environmental regulations

(ii) To design a novel integrated system comprising ORC, SOFC, GT, SRC, and WHB for retrofitting into existing marine vessels

(iii) To develop a combined system for efficient waste heat recovery from high-temperature exhaust gases, contributing to overall energy efficiency and environmental sustainability

(iv) To conduct a comprehensive thermodynamic analysis to assess the performance of the integrated system, considering various system components and cycles

(v) To conduct an extensive parametric study to analyze the system's response to variations of the current density of SOFC, superheated temperature, and pressure of working fluid of ORC, identifying optimal operating conditions and configurations

(vi) To conduct an economic analysis to estimate the payback period and net present value of the proposed system

The proposed system is aimed at presenting a novel and adaptable approach for marine vessel systems, ensuring compliance with environmental regulations. Every pairing and bottoming cycle is meticulously chosen, considering operational conditions, available installation space, and ease of use for seafarers, along with other relevant considerations.

The overall goal is to achieve enhanced energy efficiency and reduced environmental impact in marine vessel operations.

2. System Description

The proposed system's target ship is a general cargo ship that utilizes LPG as fuel. The total propulsion power of the vessel is 3,800 kW. The specifications of the modeling vessel are detailed in Table 1.

The target ship utilizes electric propulsion, powered by LPG. Figure 1 illustrates the overall configuration of the innovative system. The primary concept of this system is to generate main power using SOFC and utilize cold energy from LPG and waste heat from SOFC to produce useful work in the form of electricity. In the system design, LPG is supplied to the SOFC before reaching its working temperature, utilizing a regenerative heat exchanger. During the gasification process of LPG, a significant amount of cold energy is lost. This lost heat is harnessed in the ORC to generate additional power for the overall system.

The system includes several components:

(i) SOFC: main power generation source

(ii) ORC: utilizes cold energy from LPG to produce more power

(iii) GT and SRC: absorb waste heat from SOFC and convert it into electric power through their expander devices

(iv) WHB: captures waste heat from SOFC and transfers it to water for providing superheated steam for the purposes of accommodating and heating on board

Through this integrated design, the system is aimed at enhancing overall efficiency and power output by effectively utilizing waste heat and cold energy from LPG, thereby maximizing the energy utilization of the ship's propulsion system.

Figure 2 presents a schematic diagram of the ORC-SOFC-GT-ORC-WHB-integrated system, utilizing LPG as a heat sink. The LPG is stored in the target vessel using an IMO type C tank at a condition of 4 bars and -10°C [25, 26]. Before using LPG in fuel cells, it needs to be regasified into gas form. During this regasification process, a substantial amount of cold energy is lost. To make use of this cold energy, it is harvested in the ORC before being supplied to heat exchanger HEX-3, which raises the working temperature of the SOFC.

In the reforming process, water is introduced into the system. After regeneration in HEX-4, the water transforms into vapor and is then supplied to the propane reforming system of the SOFC through stream 7. Simultaneously, air from the ambient environment undergoes pressurization to 4 bars before being delivered to the cathode of the SOFC. To achieve the desired operating temperature of the SOFC (stream 5), the supply air (stream 4) is preheated by the heat exchanger HEX-2. Within the stack of the SOFC, the electrochemical reaction takes place, and the resulting exhaust gas is directed into the afterburner for completing the burning process.

Table 1: Vessel specification.

Items	Values
Vessel type	General cargo
Fuel type	LPG
Total propulsion power	3800 kW
Beam	13 m
Deadweight	3000 DWT
Propulsion	Electric propulsion driving
Overall length	120 m

To achieve waste heat recovery and optimize the system's output power, the integration and installation of GT and combined cycles are carried out. These cycles effectively recover the high-temperature exhaust gas and convert it into useful work, thereby significantly enhancing the overall efficiency and power generation capabilities of the integrated system.

Consequently, the high-temperature exhaust heat is effectively utilized in the SRC cycle through heat exchanger HEX-5. The power generated by the expansion device of the SRC further augments the overall power output of the system. Moreover, a waste heat boiler is integrated into the system to capture and transfer the exhaust heat to water. This process generates steam, which can serve various purposes on the vessel, such as providing accommodation for seafarers and heating lubricating oil.

The innovative ideas, methodologies, and research carried out in this study hold substantial potential to advance and promote the use of alternative fuels and green energy in maritime applications. By combining LPG with SOFCs, implementing waste heat recovery, and harnessing cold energy, the integrated system exemplifies a more efficient and environmentally friendly approach to power generation in the maritime industry.

The study's findings can significantly contribute to the progress of sustainable practices and the adoption of green technologies in the maritime sector, leading to reduced greenhouse gas emissions and fostering a more sustainable future for the shipping industry.

3. Thermodynamic Models

3.1. Thermodynamic Model Assumptions. In this section, the analysis focuses on the mass and heat balance, entropy balance, and exergy destruction rate of the system. The foundation for this analysis is based on the principles of the first and second laws of thermodynamics. To facilitate the analysis, the following main assumptions are made [27]:

(i) It is presumed that the system will function in a steady-state scenario

(ii) Any changes in kinetic and potential energy within the system are considered negligible

(iii) Heat losses that might occur in the pipelines are neglected and not considered in this analysis

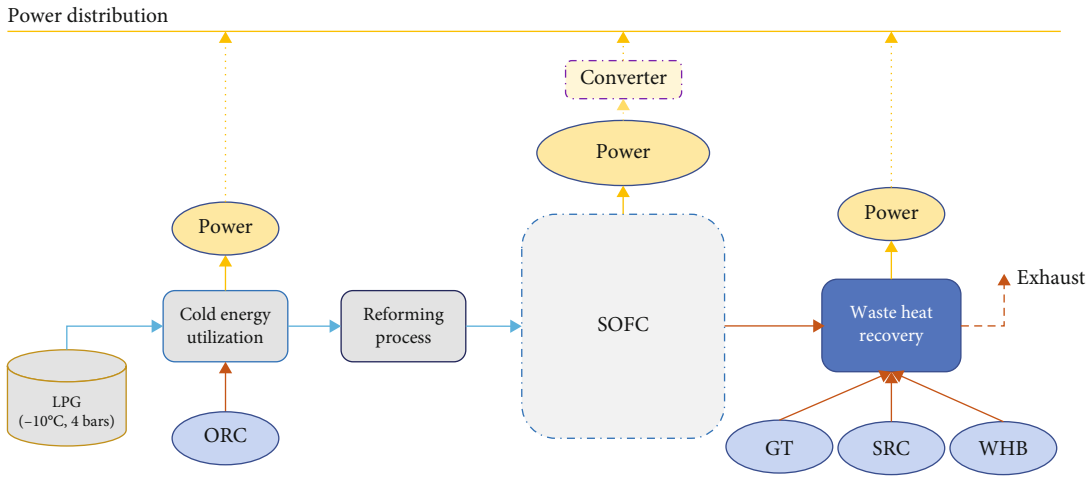

Figure 1: Block diagram of LPG SOFC-integrated system.

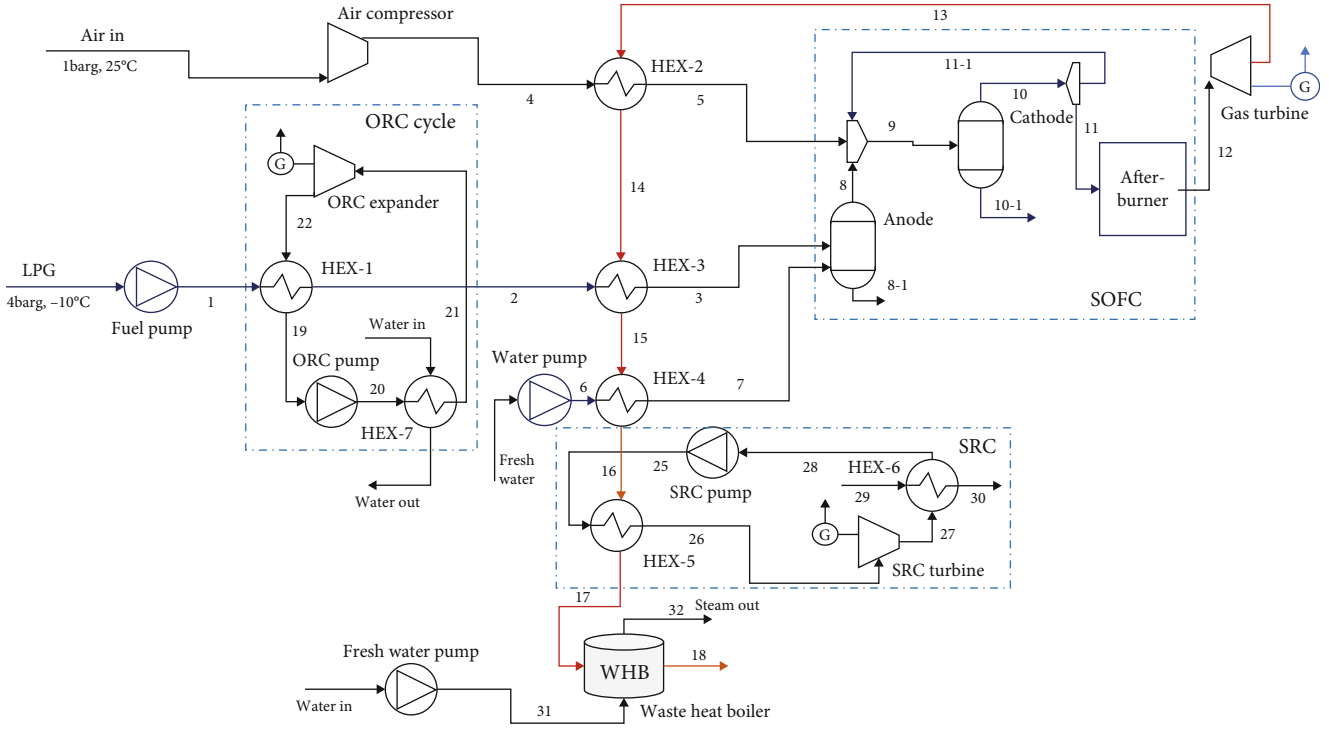

Figure 2: Schematic of the LPG ORC-SOFC-GT-SRC-integrated system.

(iv) The pressure drops in the heat exchangers are considered and assumed to be 34.47 kPa (5 psi) on the shell side and 6.895 kPa (1 psi) on the tube side. There are no pressure drops occurring within the pipelines

(v) The LPG used in the system consists of 97% C_3H_8 (propane) and 3% C_4H_{10} (n-butane).

3.2. Model of the SOFC. In the current study, the SOFC is modeled with four major considerations, which include the kinetics of electrochemical reactions, ionic and electron transport, and heat transfer. The main source of power production in the SOFC is the electrochemical reactions of oxygen and hydrogen ions [28]. However, using pure hydrogen as the primary fuel for SOFCs presents challenges, especially in maritime transportation, due to its low volumetric density, requiring large storage tanks and limited transportation distance. To overcome this challenge, the study is aimed at identifying a suitable "hydrogen carrier" fuel that contains a high hydrogen content. Moreover, since SOFCs operate at high temperatures (typically between 600 and 1000°C), LPG can undergo automatic decomposition into hydrogen inside the cell stacks.

The following equations describe the main electrochemical processes in the SOFC when using LPG as the fuel

source. These equations play a crucial role in understanding the fundamental reactions and energy conversion mechanisms occurring within the SOFC. By exploring the use of LPG as a hydrogen carrier fuel in SOFCs, the study is aimed at enhancing the feasibility and practicality of utilizing these fuel cells in various applications, including maritime transportation.

3.2.1. Reformation [29, 30]. General reaction:

$$C_nH_{2n+2} + nH_2O \leftrightarrow (2n+1)H_2 + nCO. \quad (1)$$

Propane steam reforming reaction:

$$C_3H_8 + 3H_2O \leftrightarrow 7H_2 + 3CO \quad \Delta H = 499\,\text{kJ/mol}. \quad (2)$$

Butane steam reforming reaction:

$$C_4H_{10} + 4H_2O \leftrightarrow 9H_2 + 4CO \quad \Delta H = 651\,\text{kJ/mol}. \quad (3)$$

Shifting reaction [9]:

$$CO + H_2O \leftrightarrow H_2 + CO_2 \quad \Delta H = -41\,\text{kJ/mol}, \quad (4)$$

$$2H_2 \leftrightarrow 4H^+ + 4e^-. \quad (5)$$

SOFC's electrochemical reaction [10]:

$$O_2 + 4e^- + 4H^+ \longrightarrow 2H_2O, \quad (6)$$

$$O_2 + 2H_2 \longrightarrow 2H_2O. \quad (7)$$

The temperature-dependent nature of equilibrium constants for reforming and shifting processes allows their determination through the following equation [12]:

$$\log K_p = \alpha T^4 + \beta T^3 + \gamma T^2 + \delta T + \varepsilon. \quad (8)$$

Table 2: The constant of shifting and reforming value.

	Shifting	Reforming
α	5.47301×10^{-12}	-2.63121×10^{-11}
β	-2.57479×10^{-8}	1.24065×10^{-7}
γ	4.63742×10^{-5}	-2.25232×10^{-4}
δ	-3.91500×10^{-2}	1.95028×10^{-1}
ε	1.32097×10^{1}	-6.61395×10^{1}

Based on (9) and (10), the constant of α, β, γ, δ, and ε will be presented in Table 2.

Presuming a perpetual state of equilibrium for the reforming and shifting reactions, the equilibrium constants can be computed based on the partial pressures of both reactants and products.

$$K_{p-\text{reforming}} = \frac{P_{H_2}^3 P_{CO}}{P_{C_3H_8} P_{C_4H_{10}} P_{H_2O}}, \quad (9)$$

$$K_{WGS} = \frac{P_{H_2} P_{CO_2}}{P_{CO} P_{H_2O}}. \quad (10)$$

Presuming that x, y, and z represent the molar flow rates of C_3H_8, C_4H_{10}, CO, and H_2, respectively, involved in the reactions [9]

$$K_{p-\text{reforming}} = \frac{\left([CO]^i + x - y\right)/n_{tot}^i + 2x\right)\left([H_2]^i + 3x + y - z\right)/\left(n_{tot}^i + 2x\right)}{\left([C_3H_8]^i - x\right)\left([C_4H_{10}]^i - x\right)/\left([H_2O]^i - x - y + z\right)/\left(n_{tot}^i + 2x\right)} P_{cell}^2, \quad (11)$$

$$K_{p-\text{shifting}} = \frac{\left([CO_2]^i + y\right)/n_{tot}^i + 2x\right)\left([H_2]^i + 3x + y - z\right)/\left(n_{tot}^i + 2x\right)}{\left([CO]^i + x - y\right)/\left(n_{tot}^i + 2x\right)\left([C_3H_8]^i - x\right)\left([C_4H_{10}]^i - x\right)/\left([H_2O]^i - x - y + z\right)/\left(n_{tot}^i + 2x\right)}. \quad (12)$$

Both the reforming and shifting reactions exhibit an endothermic nature, and the required heat for each reaction can be determined through

$$Q_r = x\left(h_{CO} + 3h_{H_2} - h_{H_2O} - h_{C_3H_8} - h_{C_4H_{10}}\right), \quad (13)$$

$$Q_s = y\left(h_{CO_2} + 3h_{H_2} - h_{CO} - h_{H_2O}\right). \quad (14)$$

Presuming that the heat produced through the electrochemical process within the fuel cell stack is denoted as Q_{rxn}, the overall heat available for transfer from the stack will be

$$Q = Q_{rxn} - Q_r - Q_s). \quad (15)$$

During the steam reforming process, the reaction mixture reaches an equilibrium state that involves the water-gas shift and methanation reactions. Consequently, the final product comprises a blend of CH_4, CO, H_2, CO_2, and H_2O [18]. Steam reforming is significantly affected by essential factors such as the providing temperature, quantity of steam, and space velocity of the reactants. In real-world applications of steam reforming, the actual amount of steam introduced to the hydrocarbon feed is usually much greater than what the balanced thermodynamic

equation suggests. This surplus steam is vital to prevent the hydrocarbon feed gas from breaking down and creating carbon deposits on the catalyst or reactor walls.

The quantity of steam present in the feed is typically denoted using the steam-to-carbon ratio (STCR). This proportion signifies the relationship between the moles of steam and the quantity of carbon atoms present in the hydrocarbon feed. For propane, the thermodynamic S/C ratio is 1.0, but in practice, a higher S/C ratio is often used to ensure efficient steam reforming and prevent carbon deposition issues.

Water is required for the methane reforming process. The STCR can be determined using the following calculation:

$$\mathbf{STCR} = \frac{\mathbf{q_{H_2O}}}{\mathbf{q_{LPG}}}. \tag{16}$$

The molar flow rate of water supply is represented by q_{H_2O}(mole/s), and the molar flow rate of LPG supply is represented by q_{LPG} (mole/s).

The electrochemical reaction's rate:

$$\mathbf{z} = \mathbf{U_f}(\mathbf{x} + \mathbf{3y}). \tag{17}$$

In this context, the variables are defined as follows: z represents the rate of the electrochemical reaction (mole/s), y represents the rate of the water-gas shift reaction (mole/s), x represents the rate of the reforming reaction (mole/s), and U_f represents the fuel utilization factor of SOFC.

The reforming reactions taking place within the SOFC can be delineated through Equations (2) and (3), encapsulating the processes of methane reforming and the WGS reaction.

Within the SOFC, the methane reforming and WGS reactions swiftly attain equilibrium owing to the elevated reaction temperature. The composition and concentrations of the resultant product gas mixture following the reforming reaction closely align with the equilibrium constant (K) of the reaction, a parameter solely contingent upon the reaction temperature as elucidated in Equation (8).

$$\begin{aligned} K_{p-\text{reforming}} = \frac{P_{H_2}^3 P_{CO}}{P_{C_3H_8} P_{C_4H_{10}} P_{H_2O}} &= -2.63121 \times 10^{-11}.T^4 \\ &+ 1.24065 \times 10^{-7}.T^3 - 2.25232 \times 10^{-4}.T^2 \\ &+ 0.195028.T - 66.1395, \end{aligned} \tag{18}$$

$$\begin{aligned} K_{p-\text{shifting}} = \frac{P_{H_2} P_{CO_2}}{P_{CO} P_{H_2O}} &= 5.47301 \times 10^{-12}.T^4 \\ &- 2.57479 \times 10^{-8}.T^3 + 4.63742 \times 10^{-5}.T^2 \\ &- 0.03915.T + 13.2097. \end{aligned} \tag{19}$$

3.2.2. Fuel and Air Utilization. The air/fuel utilization factor is known as the ratio of the rate of air/fuel supplied to a fuel cell divided by the rate of air/fuel consumed in the cell. It represents the efficiency of air and fuel utilization in the fuel cell system [31]:

$$\mathbf{U_{fuel}} = \frac{\mathbf{(LPG)_{reacted}}}{\mathbf{(LPG)_{supplied}}} = \frac{\mathbf{(H_2)_{reacted}}}{\mathbf{(H_2)_{supplied}}}. \tag{20}$$

Air utilization:

$$\mathbf{U_{air}} = \frac{\mathbf{(Air)_{reacted}}}{\mathbf{(Air)_{supplied}}} = \frac{\mathbf{(O_2)_{reacted}}}{\mathbf{(O_2)_{supplied}}}. \tag{21}$$

The mass flow rate [32]:

$$\mathbf{m_{SOFC,Oxygen}} = \frac{\mathbf{P_{SOFC}}}{\mathbf{U_{SOFC} \bullet n \bullet F}} \left(\frac{\mathbf{mol}}{\mathbf{min}}\right). \tag{22}$$

$$\mathbf{q_{fuel}} = \frac{\mathbf{i \bullet N_{Cell} \bullet A_{Cell}}}{\mathbf{U_f \bullet n_e \bullet F}} \left(\frac{\mathbf{mol}}{\mathbf{s}}\right). \tag{23}$$

In this context, P_{SOFC} denotes the power generated by the SOFC (kW). The variable n_e corresponds to the quantity of electrons transferred from anode to cathode of SOFC, i represents the current density of the SOFC (A/m^2), while F stands for the Faraday constant with a value of 96.458 (C/mol).

The calculation of the necessary hydrogen supply is also determined using equation (6):

$$\mathbf{m_{SOFC,hydrogen}} = \mathbf{2 \bullet m_{SOFC,Oxygen}} \left(\frac{\mathbf{mol}}{\mathbf{min}}\right). \tag{24}$$

The power output of the SOFC stack [33]:

$$W_{\text{stack}} = \text{i}.A.V_c\eta_{\text{DA}}. \tag{25}$$

In this context, V_c represents the actual voltage of the stack (V), η_{DA} is the efficiency of the DC-AC converter (%), i represents current density (A/m^2), and A is the surface area (m^2).

The current density [34]:

$$\mathbf{i} = \frac{\mathbf{z.F.n_e}}{\mathbf{N_{cell}\,A}}. \tag{26}$$

Moreover, the I-V curve is extensively employed for determining the voltage of the cell stack [35].

The electrical efficiency:

$$\eta_{\text{en,SOFC}} = \frac{\dot{W}_{\text{elect,SOFC}}}{\dot{m}_3 h_3 + \dot{m}_{\text{air}} h_{\text{air}} - \dot{m}_{11} h_{11}}. \tag{27}$$

In this context $\dot{m}_3$ represents the LPG's mass flow rate to the SOFC (kg/h), and LHV_{LPG} represents low heating value of LPG (kJ/kg).

3.2.3. Afterburner. The unreacted fuel and air remaining from the SOFC's stack electrochemical reaction are continuously combusted in an afterburner to raise the temperature and pressure of the gas turbine's intake line [36].

Table 3: Efficiency equations of the system.

Component	Energy efficiency	Exergy efficiency
GT	$\eta_{s,T} = \frac{\sum_i (\dot{n}_i \bar{h}_i)_{\text{in}} - \sum_i (\dot{n}_i \bar{h}_i)_{\text{out}}}{\sum_i (\dot{n}_i \bar{h}_i)_{\text{in}} - \sum_i (\dot{n}_i \bar{h}_i)_{s,\text{out}}}$	$\psi_T = \frac{\dot{W}_T}{\sum_i (\dot{n}_i \overline{\text{ex}}_i)_{\text{in}} - \sum_i (\dot{n}_i \overline{\text{ex}}_i)_{\text{out}}}$
SOFC-GT	$\eta_{\text{en,SOFC,GT}} = \frac{\dot{W}_{\text{SOFC}} + \dot{W}_{\text{GT}}}{\dot{m}_{\text{LPG}}\, \text{LHV}_{\text{LPG}}}$	$\eta_{\text{ex,SOFC,GT}} = \frac{\dot{W}_{\text{SOFC}} + \dot{W}_{\text{GT}}}{\dot{m}_{\text{LPG}}\, \text{ex}_{\text{LNG}}}$
Air compressor	$\eta_{\text{en,compressor}} = \frac{\sum_i (\dot{n}_i \bar{h}_i) s_{,\text{out}} - \sum_i (\dot{n}_i \bar{h}_i)_{\text{in}}}{\sum_i (\dot{n}_i \bar{h}_i)_{\text{out}} - \sum_i (\dot{n}_i \bar{h}_i)_{\text{in}}}$	$\eta_{\text{ex,compressor}} = \frac{\sum_i (\dot{n}_i \overline{\text{ex}}_i)_{\text{in}} - \sum_i (\dot{n}_i \overline{\text{ex}}_i)_{\text{out}}}{\dot{W}_C}$
ORC	$\eta_{\text{en,ORC}} = \frac{\dot{W}_{\text{net,ORC}}}{\dot{Q}_{\text{in,ORC}}}$	$\eta_{\text{ex,ORC}} = \frac{\dot{W}_{\text{net,ORC}}}{\dot{\text{E}}\text{x}_{\text{in,ORC}}}$
SRC	$\eta_{\text{en,SRC}} = \frac{\dot{W}_{\text{elec,SRC}}}{\dot{m}_{16}(h_{16} - h_{17})}$	$\eta_{\text{ex,SRC}} = \frac{\dot{W}_{\text{elec,SRC}}}{\dot{m}_{16}(\text{ex}_{16} - \text{ex}_{17})}$

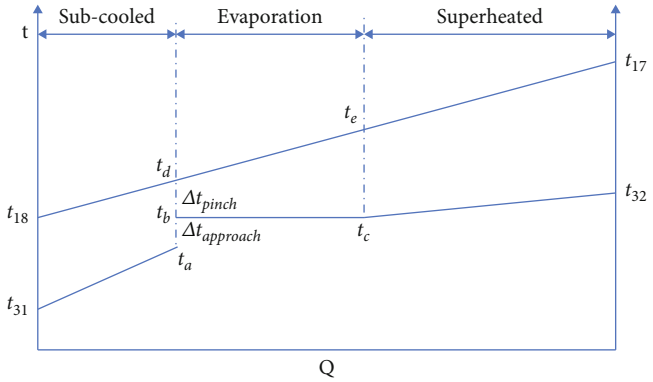

Figure 3: Temperature zone for WHB.

$$O_2 + 2CO \longrightarrow 2CO_2, \tag{28}$$

$$O_2 + 2H_2 \longrightarrow 2H_2O. \tag{29}$$

The estimation of heat loss at the afterburner is performed by

$$\mathbf{Q_{loss,afterburner}} = \mathbf{q_{LPG}}\,(\mathbf{1} - \mathbf{U_f})(\mathbf{1} - \boldsymbol{\eta}_{\mathbf{afterburner}})\mathbf{LHV}. \tag{30}$$

In this context, $Q_{\text{loss,afterburner}}$ represents heat loss by afterburner (kW).

The equations for estimation of the system performances (energy efficiency and exergy efficiency) are presented in Table 3.

3.3. Waste Heat Boiler. In this context, the exhaust heat boiler plays a vital role in providing hot steam and water to accommodate seafarers working on board the ship. The waste heat boiler functions by recovering heat from the flue gas through the boiler drum, resulting in the generation of hot steam. The estimated steam is produced at a temperature of 151°C, a pressure of 499 kPa, and a rate of 8,200 kg/h. The operation of the exhaust gas boiler is divided into three distinct regions, namely, single-phase subcooled, two-phase evaporation, and single-phase superheated, as depicted in Figure 3. The heat balance of this system is carefully considered to ensure efficient operation.

Table 4: Equations for exergy destructions.

Components	Exergy destruction rate
SOFC	$\dot{\mathbf{E}}\mathbf{x}_2 + \dot{\mathbf{E}}\mathbf{x}_4 + \dot{\mathbf{E}}\mathbf{x}_{11-1} - \dot{\mathbf{E}}\mathbf{x}_{11} - \dot{\mathbf{W}}_s = \dot{\mathbf{E}}\mathbf{x}_{\mathbf{des}}$
Afterburner	$\dot{\mathbf{E}}\mathbf{x}_{11} - \dot{\mathbf{E}}\mathbf{x}_{12} = \dot{\mathbf{E}}\mathbf{x}_{\mathbf{des}}$
Gas turbine	$\dot{\mathbf{E}}\mathbf{x}_{12} - \dot{\mathbf{E}}\mathbf{x}_{13} - \dot{\mathbf{W}}_{\mathbf{Gas\,turbine}} = \dot{\mathbf{E}}\mathbf{x}_{\mathbf{des}}$
HEX-1	$\dot{\mathbf{E}}\mathbf{x}_1 + \dot{\mathbf{E}}\mathbf{x}_{22} - \dot{\mathbf{E}}\mathbf{x}_2 - \dot{\mathbf{E}}_{19} = \dot{\mathbf{E}}\mathbf{x}_{\mathbf{des}}$
HEX-2	$\dot{\mathbf{E}}\mathbf{x}_{13} + \dot{\mathbf{E}}\mathbf{x}_4 - \dot{\mathbf{E}}\mathbf{x}_5 - \dot{\mathbf{E}}_{14} = \dot{\mathbf{E}}\mathbf{x}_{\mathbf{des}}$
ORC expanders	$\dot{\mathbf{E}}\mathbf{x}_{21} - \dot{\mathbf{E}}\mathbf{x}_{22} - \dot{\mathbf{W}}_{\mathbf{OC\_Turbine}} = \dot{\mathbf{E}}\mathbf{x}_{\mathbf{des}}$
HEX-3	$\dot{\mathbf{E}}\mathbf{x}_{14} + \dot{\mathbf{E}}\mathbf{x}_2 - \dot{\mathbf{E}}\mathbf{x}_3 - \dot{\mathbf{E}}_{15} = \dot{\mathbf{E}}\mathbf{x}_{\mathbf{des}}$
HEX-4	$\dot{\mathbf{E}}\mathbf{x}_{15} + \dot{\mathbf{E}}\mathbf{x}_6 - \dot{\mathbf{E}}\mathbf{x}_7 - \dot{\mathbf{E}}_{16} = \dot{\mathbf{E}}\mathbf{x}_{\mathbf{des}}$
HEX-5	$\dot{\mathbf{E}}\mathbf{x}_{16} + \dot{\mathbf{E}}\mathbf{x}_{25} - \dot{\mathbf{E}}\mathbf{x}_{17} - \dot{\mathbf{E}}_{26} = \dot{\mathbf{E}}\mathbf{x}_{\mathbf{des}}$
HEX-6	$\dot{\mathbf{E}}\mathbf{x}_{27} + \dot{\mathbf{E}}\mathbf{x}_{29} - \dot{\mathbf{E}}\mathbf{x}_{28} - \dot{\mathbf{E}}_{30} = \dot{\mathbf{E}}\mathbf{x}_{\mathbf{des}}$
HEX-7	$\dot{\mathbf{E}}\mathbf{x}_{18} + \dot{\mathbf{E}}\mathbf{x}_{20} - \dot{\mathbf{E}}\mathbf{x}_{21} - \dot{\mathbf{E}}_{23} = \dot{\mathbf{E}}\mathbf{x}_{\mathbf{des}}$
Exhaust heat boiler	$\dot{\mathbf{E}}\mathbf{x}_{17} + \dot{\mathbf{E}}\mathbf{x}_{31} - \dot{\mathbf{E}}\mathbf{x}_{32} - \dot{\mathbf{E}}_{18} = \dot{\mathbf{E}}\mathbf{x}_{\mathbf{des}}$
SRC-Turbine	$\dot{\mathbf{E}}\mathbf{x}_{26} - \dot{\mathbf{E}}\mathbf{x}_{27} - \dot{\mathbf{E}}\mathbf{x}_{\mathbf{SRC-Turbine}} = \dot{\mathbf{E}}\mathbf{x}_{\mathbf{des}}$

(i) Superheated zone:

$$\dot{m}_{17}(h_{17} - h_e) = \dot{m}_{31}(h_{32} - h_c). \tag{31}$$

(ii) Evaporation zone:

$$\dot{m}_{17}(h_e - h_d) = \dot{m}_{31}(h_c - h_a). \tag{32}$$

(iii) Subcooled zone:

$$\dot{m}_{17}(h_d - h_{18}) = \dot{m}_{31}(h_a - h_{31}). \tag{33}$$

(iv) The total heat transferred:

$$Q = U \cdot A \cdot \text{LMTD}. \tag{34}$$

Table 5: The designation and input data of the system.

Component	Parameter	Unit	Value
SOFC	Operating pressure	bar	4.00
	Number of single cells		16804
	Operating temperature	˚C	866.4
	Active surface area	m^2	0.22
	Cell voltage	V	0.735
	Electron number		2
	Fuel cell current density	A/m^2	1427
	Oxygen stoichiometric		1.8
	Cathode thickness	cm	0.003
	Hydrogen stoichiometric		1.1
	Anode thickness	cm	0.003
	Fuel utilization factor in SOFC		90%
	Stack power output	V	226.131
	Electrolyte thickness	cm	0.01
Compressor, expanders, and pumps	Isentropic efficiency	%	88
Converter	DC-AC converter efficiency	%	97

Table 6: The comparison between current system and literature.

Parameter	Current study	Literature 1	
		Reported [37]	Difference
SOFC temperature (˚C)	866.4	870	0.41%
Current density (A/m^2)	1427	1429	0.13%
Cell voltage (V)	0.735	0.747	1.61%
Gas turbine inlet temperature (˚C)	1179	1201	1.83%
SOFC efficiency	40.47	50.96	10.49%

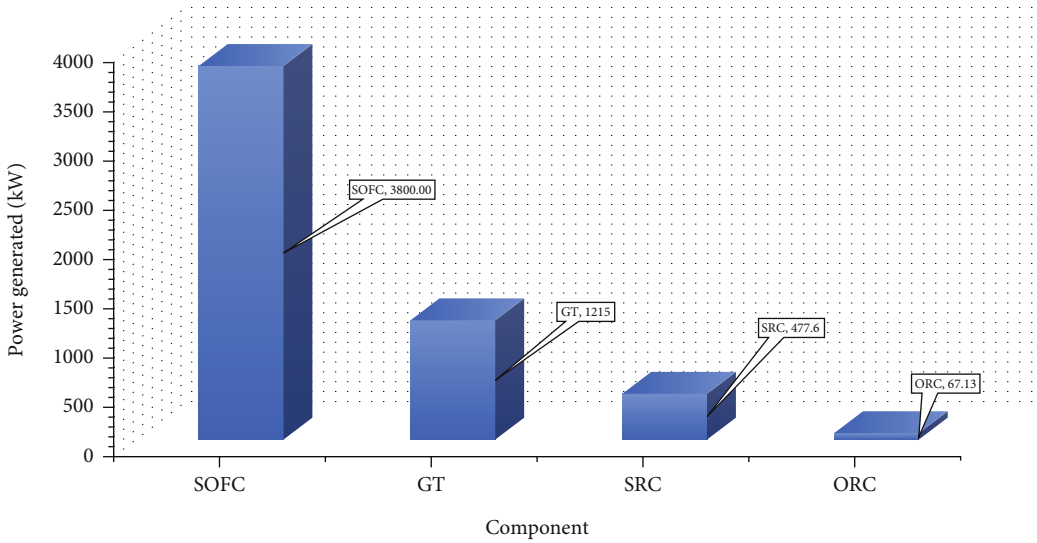

Figure 4: Power produced by major components of suggested system.

in which LMTD, A, and U represent logarithmic mean temperature difference, heat exchange area (m^2), and heat exchange coefficient ($30\,W m^{-2} K^{-1}$).

$$\mathrm{LMTD} = \frac{\Delta T_{2,\mathrm{end}} - \Delta T_{1,\mathrm{end}}}{\ln\left(\Delta T_{2,\mathrm{end}}/\Delta T_{1,\mathrm{end}}\right)}. \tag{35}$$

The temperature difference of hot and cold end is represented by $\Delta T_{1,\mathrm{end}}$ and $\Delta T_{2,\mathrm{end}}$.

Based on the first and second laws of thermodynamics, the exergy equation is built for developed system (see in Table 4).

The performance of the integrated system is computed through the following.

Energy efficiency:

$$\boldsymbol{\eta_{\mathrm{en,overall}}} = \frac{\dot{\mathbf{W}}_{\mathbf{elec,system}}}{\dot{\mathbf{m}}_{\mathbf{LPG}}\,\mathbf{LHV_{LPG}}}. \tag{36}$$

In this context, $\dot{W}_{\mathrm{elec,system}}$ is calculated by

$$\begin{aligned}\dot{W}_{\mathrm{elec,total}} = {} & \dot{W}_{\mathrm{elec,SOFC}} + \dot{W}_{\mathrm{Gas\ turbine}} + \dot{W}_{\mathrm{SRC,turbine}} \\ & + \dot{W}_{\mathrm{ORC}} - \dot{W}_{\mathrm{Air\ comp}} - \dot{W}_{\mathrm{SRC,pump}} \\ & - \dot{W}_{\mathrm{ORC,pump}} - \dot{W}_{\mathrm{Fresh\ water\_P}}.\end{aligned} \tag{37}$$

$\mathrm{LHV_{LPG}}$ represents the lower heating value of LPG (kJ/kg).

The exergy efficiency:

$$\eta_{\mathrm{ex,overall}} = \frac{\dot{W}_{\mathrm{elec,total}}}{\dot{m}_{\mathrm{LPG}}\,\mathrm{ex_{LPG}}}. \tag{38}$$

4. Simulation Materials

The proposed system, which combines ORC, SOFC, GT, SRC, and EHB, utilizes LPG (liquefied petroleum gas) as the fuel. The design and simulation of this system are conducted using ASPEN HYSYS V12.1, a software developed by Aspen Technology Inc. (Massachusetts, US). To analyze the thermal properties of each node in the system, Aspen HYSYS utilizes REFPROP as its physical property system. The Peng-Robinson (PR) equation of state is chosen to estimate the thermodynamic states and compositions of various points within the system.

During the simulation process, the following assumptions are considered:

(1) The condition of air inlet is at 29.85°C and 101.3 kPa

(2) The air is assumed to consist of 79% N_2 and 21% O_2

The specified input parameters to the proposed system are presented in Table 5.

4.1. Modeling Verification. In order to corroborate the existing nomenclature, the current findings are cross-referenced with the data published by Liu et al. [37], as demonstrated in Table 6. The obtained results exhibit favorable concordance with the literature data, and discrepancies in comparative analysis are maintained within acceptable limits.

Table 7: System's indicators.

Subsystem	Energy efficiency (%)	Exergy efficiency (%)
SOFC	40.47	
SOFC-GT	47.04	45.65
SRC	31.88	30.23
ORC	28.24	29.21
Total integrated system	52.65	51.10

In comparison with other fuel types [12, 32, 38, 39] and reported model [37] by LNG, the LPG system showed lower performance efficiency [20, 22]. This can be explained by more longer and complicated reformation procedure of LPG inside the SOFC [40] resulting in the uncompleted electrochemical reaction inside SOFC [18]. The efficiency of LPG SOFC can be increased by the participation of appropriate catalyst materials [41, 42]. Besides, the integration of the exhaust heat boiler has been proven to keep an important role in supplying superheated vapor for various purposes such as sailors' accommodation and serving as a heating medium for fuel and oil. The indispensability of waste heat recovery is substantiated by its substantial contribution of 31.65% towards the total power output.

5. Results and Discussions

5.1. The Performances of System. The primary motive force of the target vessel necessitates 3800 kW, and an additional 1759.73 kW of surplus of power is of utmost importance to cater to the hotel loads, encompassing auxiliary machinery, and the accommodation facilities for seafarers. In the foundational scenario, employing a SOFC operating at a cell voltage of 0.735 V and a current density of 1427 A/m^2 yielded an exceptional electrical efficiency of 40.47%. The seamless integration of this combined system demonstrated remarkable prowess, culminating in a total power output of 5559.73 kW (as in Figure 4). This ingeniously devised system is adeptly designed to encompass both combined cycles, effectively harnessing the latent cold energy of LPG and recovering waste heat.

Conducting an astute performance analysis, it is evident that the SOFC contributes substantially, generating 68.35% of the entire power output, while the combined cycle plays its part, contributing 31.65% (as in Table 7). Notably, the surplus power generated by this integrated marvel exquisitely satisfies the energy requisites of auxiliary machinery, illuminative elements, pumping systems, and the indispensable habitation needs of seafarers, seamlessly meeting the propulsive exigencies of the main power plant.

The overall system's energy and exergy efficiencies are calculated to be 52.65% and 51.10%, respectively.

Among the integrated cycles, the SRC subsystem illustrated performances of 31.88% and 30.23% of energy and exergy efficiencies, respectively. In comparison with the SOFC stand-alone system, the integrated GT as waste heat recovery support 1215 kW of output power which is

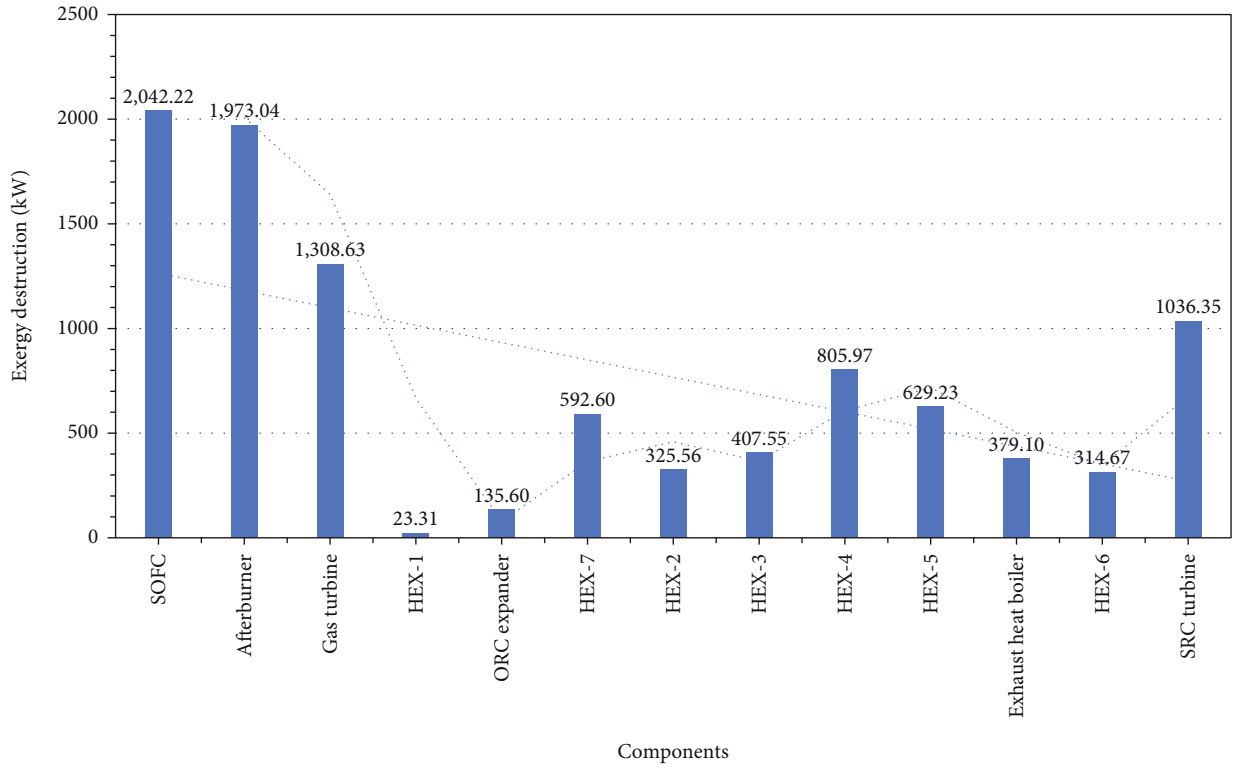

Figure 5: Exergy destruction rate of major component material stream.

equivalent to a 6.57% increase of energy efficiency. The ORC indicated high performances of energy efficiency and exergy efficiency at 28.24% and 29.21%, respectively. The reason is that the ORC capitalizes on both the low-temperature energy from the condenser and the high-temperature exhaust heat from the evaporator, leading to a larger efficiency area. As a consequence, the working fluid may reach critical pressures and temperatures, resulting in a greater power output from the fuel cell system.

Figure 5 illustrates the distribution of exergy degradation, with the most prominent contribution stemming from the SOFC, amounting to 2,042.22 kW. This significant exergy destruction can be primarily attributed to the inherent irreversibility associated with the electrochemical reactions occurring within the SOFC. Subsequently, the afterburner ranks as the second-highest contributor, accounting for 1,973.04 kW of exergy destruction, affirming its efficacy in promoting complete combustion of fuel and air within the SOFC system. In succession, the GT and the SRC expander contribute 1,308.63 and 1,036.35 kW, respectively, to the overall exergy destruction.

Among the heat exchangers, HEX-4 exhibits the highest exergy destruction at 805.97 kW, primarily due to the pronounced temperature disparity between the hot and cold sources within HEX-4. Moreover, HEX-4 facilitates the vaporization and phase change of water by absorbing heat from the SOFC exhaust gas, leading to elevated exergy destruction in comparison to other heat exchangers. Similarly, HEX-5, HEX-7, and HEX-3 demonstrate substantial exergy destruction owing to their capacity to recuperate high-temperature exhaust heat, resulting in significant temperature differentials between the hot and cold sources.

The SRC evaporator effectively utilizes the SOFC exhaust gas as a hot source to vaporize the working fluid, and consequently, the energy harnessed by the working fluid in the SRC expander is proficiently converted into useful electricity production.

Lastly, the exhaust heat boiler incurs notable exergy destruction of 379.10 kW due to direct heat exchange and water evaporation within the device, accentuating its significant role as a contributor to exergy losses in the system.

By the process modeling, the indicator of each node of proposed system is presented in Table 8.

5.2. Organic Rankine Cycle (ORC). Achieving the condensation of the working fluid in the ORC at a low-temperature condition is crucial to ensure alignment with both the LPG gasification curve and the condensation curve of the working fluid. For marine vessel applications, it is imperative that the selection of working fluids conforms to the requirements specified by international regulations and standards. To this end, references from authoritative sources such as the American Society of Heating, Refrigerating, and Air-Conditioning Engineers (ASHRAE), Korea Register (KR), and relevant prior research papers [43–45] were consulted. Based on these references, six suitable working fluid candidates were recommended and subsequently selected, as detailed in Table 9.

In Figure 6, the efficient recovery of waste heat from the SOFC in the evaporator of the ORC and the utilization of cold energy from the LPG in the ORC condenser result in

Table 8: The material streams.

Node Unit	Vapor fraction	Temperature C	Pressure kPa	Molar flow kgmole/h	Mass flow kg/h	Mass enthalpy kJ/kg
Air in	1.00	29.85	101.30	417.82	12054.21	4.63
Fresh water	0.00	29.85	101.00	102.30	1842.90	-15866.90
LPG	0.00	-10.00	400.00	59.05	2628.81	-2806.42
1	0.00	-9.96	450.00	59.05	2628.81	-2806.29
2	1.00	0.90	443.11	59.05	2628.81	-2403.08
3	1.00	427.00	436.21	59.05	2628.81	-1345.68
4	1.00	203.36	400.00	417.82	12054.21	183.31
5	1.00	427.00	393.11	417.82	12054.21	423.28
6	0.00	29.88	400.00	102.30	1842.90	-15866.50
7	1.00	250.00	393.11	102.30	1842.90	-13001.60
8	1.00	371.24	393.11	161.35	4471.71	-6149.37
9	1.00	425.45	393.11	617.68	17395.71	-1355.20
10	1.00	866.38	393.11	770.19	17395.68	-1355.20
11	1.00	866.38	393.11	731.68	16525.89	-1355.20
12	1.00	1179.50	393.11	713.13	16525.86	-1355.20
13	1.00	1032.98	190.00	713.13	16525.86	-1619.97
14	1.00	934.19	155.53	713.13	16525.86	-1795.01
15	1.00	837.63	121.05	713.13	16525.86	-1963.22
16	1.00	648.90	86.58	713.13	16525.86	-2282.70
17	1.00	362.77	52.10	713.13	16525.86	-2738.93
18	1.00	174.81	51.10	713.13	16525.86	-3017.43
19	0.00	0.00	500.00	48.00	3170.42	-7558.38
20	0.00	1.83	5000.00	48.00	3170.42	-7553.59
21	1.00	150.00	4993.11	48.00	3170.42	-7147.83
22	1.00	30.92	534.47	48.00	3170.42	-7224.05
23	1.00	119.91	16.63	713.13	16525.86	-3095.27
25	0.00	71.33	12000.00	166.53	3000.00	-15677.01
26	1.00	323.65	11993.11	166.53	3000.00	-13163.82
27	0.79	111.32	150.00	166.53	3000.00	-13736.98
28	0.00	70.00	115.53	166.53	3000.00	-15693.31
29	0.00	20.00	100.00	2775.45	50000.00	-15909.39
30	0.00	47.20	93.11	2775.45	50000.00	-15792.01
31	0.00	20.00	500.00	444.07	8000.00	-15909.01
32	0.00	151.00	499.00	444.07	8000.00	-15333.71

the maximization of the cycle's performance. Consequently, the ORC achieves its maximum output power under these conditions.

In Figures 6(a) and 6(b)), the variations of the ORC's power output, energy efficiency, and exergy efficiency are depicted concerning different superheated temperatures and evaporation pressures of the ORC's working fluid.

The cycle's cooling energy efficiency rises with increasing turbine intake temperature, while the evaporation pressure remains constant. Conversely, when the turbine intake temperature is fixed, there exists an ideal evaporation pressure of 5000 kPa that allows for the highest possible output efficiency of 36.66%. The reason behind this phenomenon is primarily attributed to the fact that alterations in cooling energy efficiency are mostly governed by net power production. Moreover, after determining the LPG cold exergy, elevating the turbine inlet temperature effectively reduces temperature disparities during heat transfer, leading to significant improvements in net output power and cold exergy efficiency.

Table 9: Condensation temperature of working fluid's candidate.

Working fluid	R32	R143a	R134a	R152a	R1150	R290
Condense temp. (°C)	-50.1	-45.4	-24.3	-22.7	-102.7	-40.3
GWP	675	4470	1430	124	4	3
ODP	0	0	0	0	0	0

As the evaporation pressure increases, the heat efficiency and net production power exhibit parabolic variations. This behavior arises from the interplay between

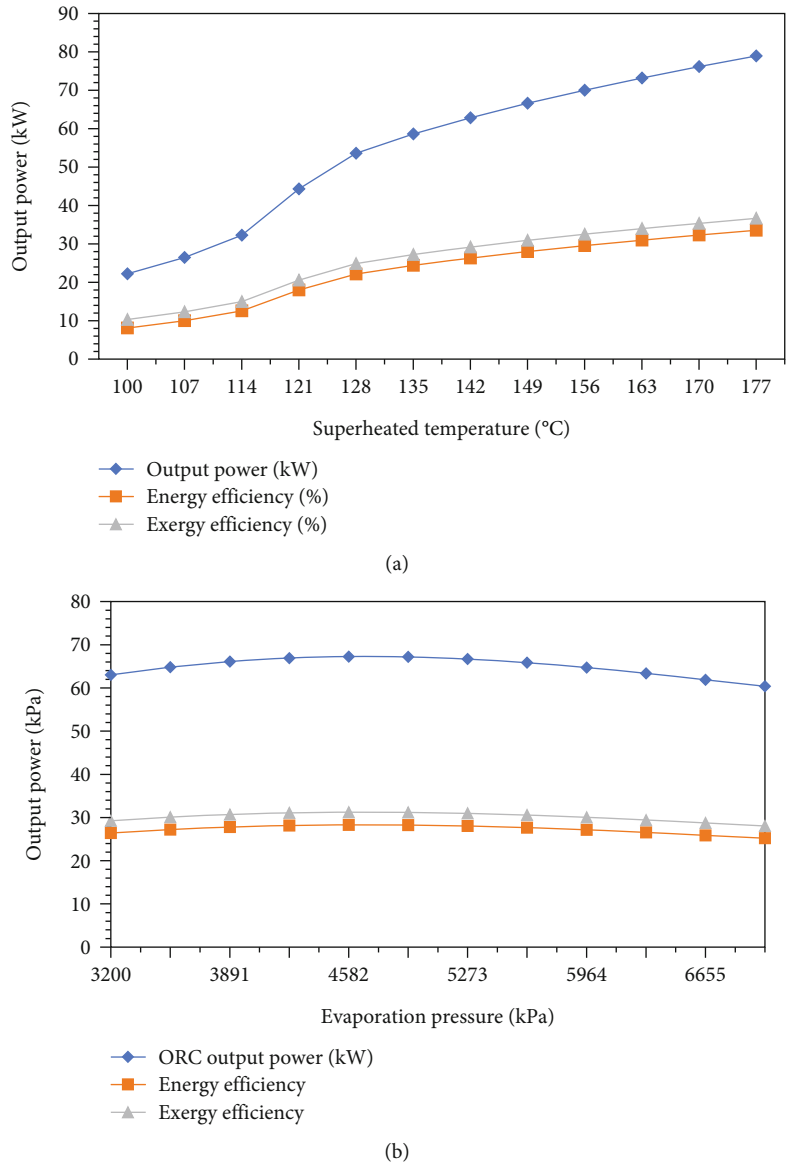

Figure 6: (a) The changes in power output and efficiencies of ORC at various superheated temperatures. (b) The ORC's power output and efficiencies under varying superheated pressure conditions.

the cycle's heat absorption and total production power, which collectively influence the thermal efficiency. However, caution is required when dealing with higher pressures, as at 5618 kPa, water may form at the expander's inlet, leading to potential damage to the turbine blade and subsequent reduction in the expander and system's performance.

When the evaporation pressure surpasses 3200 kPa, the proportional increase in power exceeds the rise in heat absorption within the ORC, resulting in enhanced thermal efficiency. On the other hand, the thermal efficiency declines when the rate of heat absorption surpasses the growth in electricity generation.

Furthermore, with a fixed evaporation pressure, higher turbine intake temperatures correspond to greater net output power and increased thermal efficiency. This effect is due to a significant reduction in heat transfer temperature differentials as the turbine intake temperature rises, thereby minimizing energy waste and considerably boosting thermal efficiency and total power production.

5.3. Effect of Current Density of SOFC. As the current density in the SOFC is varied from 900 to 1950 A/m^2, the cell voltage decreases from 0.89 to 0.48 V. Interestingly, despite the decrease in cell voltage, the power output of the SOFC increases as the current density increases. Over the examined range of current density, the system's output power experiences a significant increase of 912.41 kW, rising from 3817.46 to 4729.87 kW. This phenomenon can be attributed to the concurrent increase in exhaust gas temperature and the mass flow rate of hydrogen supplied to the SOFC, which elevates the power generation from 2938.25 to 3900 kW.

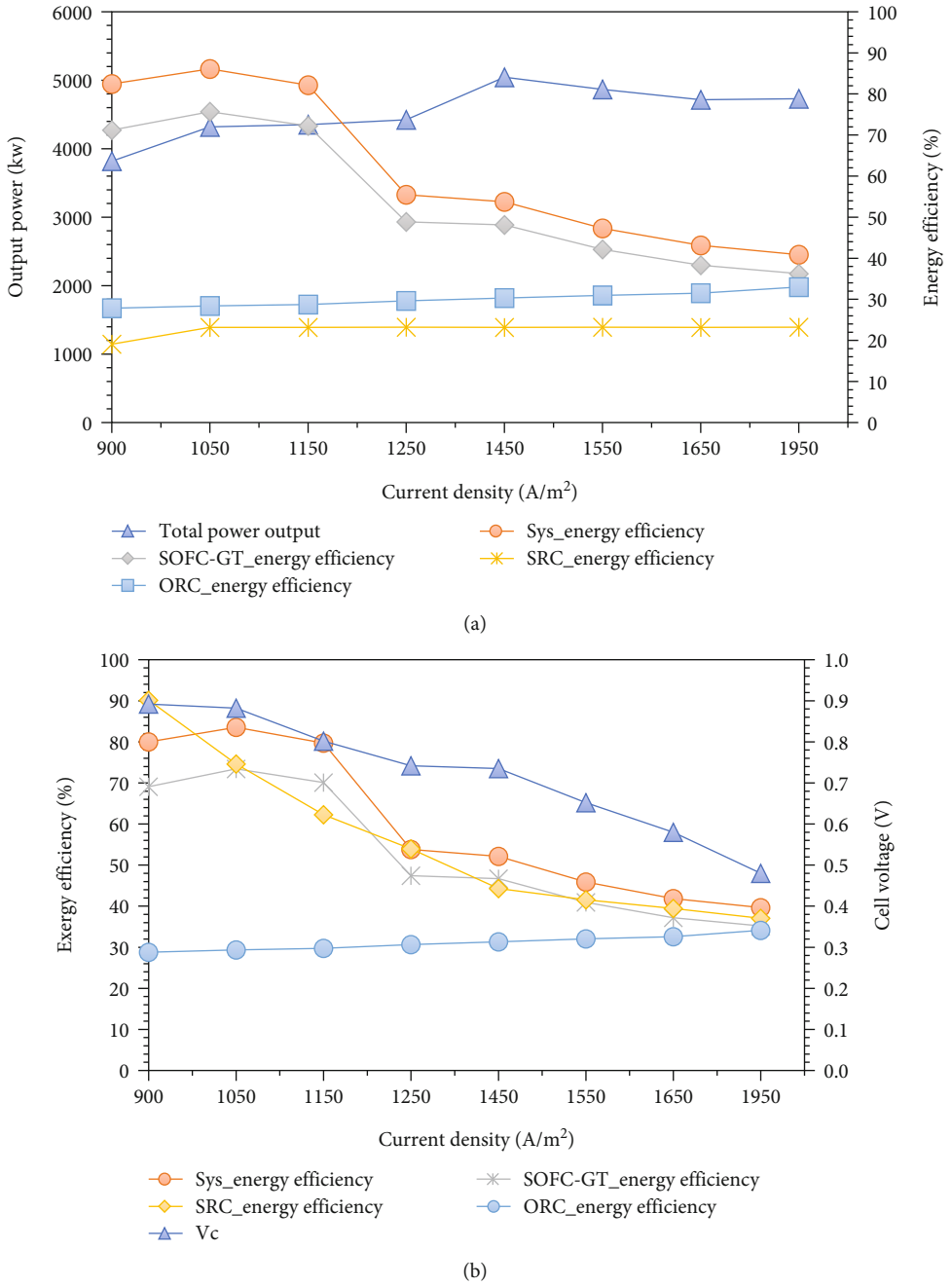

Figure 7: (a) The impact of SOFC current density on energy efficiency and power output. (b) The impact of SOFC current density on exergy efficiency and cell voltage.

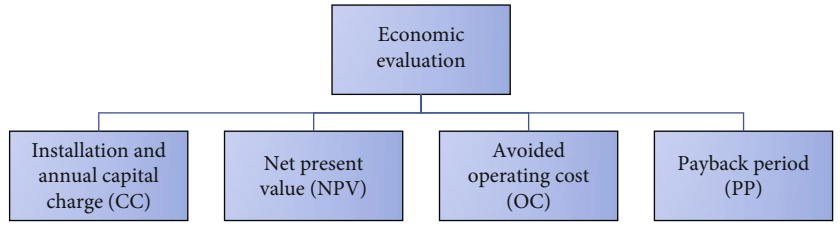

Figure 8: Scheme for economic evaluation of described system.

Table 10: The economic evaluation for ORC-SOFC-GT-SRC-WHB [37, 47, 48].

Investment component	Value
CC (million USD)	
SOFC	$CC_{SOFC} = A_{SOFC}\,(2.96T_{SOFC} - 1907)$
Heat exchangers	$CC_{HX} = 8500 + 409\,HXA^{0.8}$
Gas turbine	$CC_{GT} = \left(-98.328\ln\left(\dot{W}_{GT}\right) + 1318.5\right)\dot{W}_{GT}$
Air compressor	$CC_{Air\,comp} = \frac{39.5\,\dot{m}_a}{0.9 - \eta_{AC}}\left(\frac{P_{dc}}{P_{suc}}\right)\ln\left(\frac{P_{dc}}{P_{suc}}\right)$
Afterburner [49]	$AB_{CC} = \frac{46.8\,\dot{m}_{14}}{0.995 - P_{15}/P_{CC_{14}}}\,(1 + \exp\,(0.018T_{10} - 26.4)]$
ORC	$CC_{ORC} = 2.345.000\left(\frac{\dot{W}_{net,ORC}}{1115\,kW}\right)^{0.867}$
OC (million USD)	
Integrated system	0.05 CC
LPG price	Subsidized 1.7 {3.05%}–unsubsidized 2.9 {0.6%} USD/ton
CO_2 emission rate	$0.18\,\frac{kgCO_2}{kW.h}$
Water price unit	Subsidized 1.1 {3.1%}–unsubsidized 1.9 {0.6%} USD/m^3
Specific CO_2 emission	$\text{Specific}\,CO_2 = \frac{1}{\text{Fuel cell load}}\sum_i (CO_2)_i$
Plant availability	7800 h/year
Real discount rate	5%
Plant lifetime	25 years

However, with the increasing current density from 900 to 1950 A/m^2, the overall energy efficiency of the entire system decreases from 82.45% to 40.86%. Similarly, within the SOFC-GT subsystem, the energy efficiency also decreases by 34.93%, ranging from 71.18% to 36.25%, following the mentioned trend of current density. This reduction in efficiency is a result of the necessity to increase the mass flow rate of LPG from 360 to 900 kg/h to maintain the power output of the SOFC at the designated value. As a result, the enthalpy of the flue gas stream is modified, especially within and outside regenerative heat exchangers, due to changes in exhaust gas flow rate and parameters caused by the augmented fuel supply mass flow rate. Consequently, the efficiency of waste heat harvesting is adjusted, leading to an increase in the heating cogeneration effectiveness of the SRC system by 4.12%, from 19.08% to 23.20%.

In Figure 7(b)), the impact of the SOFC's current density on the systems' exergetic efficiency and the bulk flow rate of LPG delivery to the SOFC is depicted. The graph illustrates that as the current density increases, the overall system's energy efficiency decreases, while the mass flow rate of LPG delivery to the SOFC increases. This behavior is attributed to the interplay between changing current densities and the associated voltage losses, which affect the overall cell voltage.

Upon analyzing current densities ranging from 900 to 1950 A/m^2, it becomes evident that the system's overall exergy efficiency declines from 80.01% to 39.66%. Specifically, within this range of current densities, the exergy efficiency of the SOFC-GT decreases by 17.15%, ranging from 69.07% to 23.20%. The reduction in efficiency occurs due to intricate interplays among the SOFC's current density, voltage losses, and the overall performance of the system.

5.4. Economic Evaluation. Utilizing statistical information and data derived from the overall investment capital of the integrated system, an assessment is conducted on the economic feasibility of the combined ORC-SOFC-GT-SRC-WHB system. This evaluation encompasses installation costs, annual capital charges (CC), avoided annual operating costs (OC), net present value (NPV), payback period (PP), and discounted payback time (as in Figure 8). The objective is to ascertain the economic viability of the integrated system, specifically designed for cogenerating electricity and steam to meet the needs of seafarer's accommodation.

The initial investment expenses associated with the installation of SOFC, gas turbines, steam turbines, heat exchangers, pumps, and waste heat boilers are considered, with the assumption of no capital salvage value. The avoided annual operating costs (OC) encompass the reduction in expenses related to the purchase of LPG and the cost of CO_2 emissions, achieved through electrical power generation using the hybrid SOFC-GT system compared to a 29% efficient GT plant with equivalent net power output. Additionally, the avoided cost includes savings from not purchasing centralized network water, thanks to on-site superheated steam generation using SOFC-GT waste heat.

Fuel savings are translated into fuel-saving costs, often referred to as annual profits, and the price of LPG is a crucial factor in this calculation. Referring to literature [46], the cost

of imported LPG from Panama, Saudi Arabia, Australia, and Canada to South Korea is documented as 687, 683, 633, and 658 USD per ton, respectively. For the purpose of this economic analysis, we have considered the cost of LPG as 650 USD per ton.

The net present value (NPV) is computed through

$$\mathrm{NPV} = \sum_{i=0}^{k} \frac{R_i}{(1+a)^i}. \tag{39}$$

Within this context, a represents the actual discount rate, i signifies the investment period in years, k denotes the total number of periods, and R_i corresponds to the net cash inflow during the specified period.

The duration required for the net income from the system to recuperate the initial investment cost, referred to as the discounted payback time, is determined by the number of periods until the NPV becomes positive. The economic investment metrics for the proposed system are detailed in the following Table 10.

CC [50] is calculated by

$$\text{Annual capital charge} = \mathrm{CC}\,\frac{i}{1-(1+i)^{-t}}. \tag{40}$$

i represents the interest rate.

The period required for the system's net income to recover the initial investment cost is determined by

$$\mathrm{PP} = \frac{\text{The capital cost of power plant}}{\text{Annual income from selling electricity}} = \frac{\mathrm{CC}}{F}. \tag{41}$$

Considering subsidized and unsubsidized water/gas prices, the reductions in net annual operating costs range from 8.2 to 12.7 million USD, leading to associated end-of-life NPV ranging from 40.7 to 53 million USD. The discounted payback period is calculated to be between 8.5 and 11.2 years for unsubsidized and subsidized utility costs, respectively. In summary, the proposed integration technique of SOFC-GT and waste heat boiler demonstrates significant potential, as indicated by the conducted thermodynamic and economic feasibility analyses.

6. Conclusions

In conclusion, this pioneering study sets sail towards a greener horizon for marine vessels, showcasing the promising integration of LPG and SOFC technology. With an eye on sustainability and adaptability, this work marks the compass point for a new era in marine propulsion, where reduced emissions and enhanced efficiency become the wind in our sails, navigating us towards a more environmentally conscious and technologically advanced maritime future. The study proposes an integrated system for marine vessels, which combines a SOFC with LPG cold energy utilization and waste heat recovery mechanisms. To evaluate the system's performance, thermodynamic analysis methods and advanced modeling software are employed. The main findings and outcomes of this study are summarized as follows:

(1) The study presents a novel concept of integrating the SOFC with LPG cold energy utilization and waste heat recovery systems. This integration is aimed at enhancing the overall energy efficiency and power generation capabilities of the marine vessel. In comparison to stand-alone SOFC systems, the integrated combined system exhibits significant improvements in both total energy and exergy efficiencies. The combined system achieved 52.65% total energy efficiency and 51.10% exergy efficiency, representing an impressive 12.18% increase in energy efficiency when compared to the SOFC stand-alone systems. The integrated system, consisting of ORC, GT, SRC, and WHR contributes significantly to the overall power supply. Specifically, this combined system generated and supplied 1,759.73 kW, which accounts for 31.65% of the entire system's total power output. This demonstrates the enhanced power generation capabilities and efficiency achieved through the integration of different energy conversion mechanisms

(2) The parametric analysis showed that as the current density varied from 900 to 1,950 A/m^2, both energy efficiency and exergy efficiency of the system experienced significant reductions of 41.59% and 40.35%, respectively. Despite this decrease in efficiencies, the total power output of the system notably increased, reaching 1,227.3 kW within the tested range of current density. This could be attributed to changes in other system parameters, such as the exhaust gas temperature, hydrogen mass flow rate, or other operational adjustments, which led to the increase in total power output despite the drop-in efficiency

(3) The WHB is proficient in fulfilling various onboard ship requirements, including heating lubricating oil, machinery, and providing comfort for seafarers. It achieves this by generating 8,200 kg/h of superheated vapor at a temperature of 151°C and a pressure of 499 kPa. This ensures an adequate and reliable supply of superheated vapor to meet the ship's operational and accommodation needs

(4) By the economic evaluation, the discounted payback period is calculated to be between 8.5 and 11.2 years for unsubsidized and subsidized utility costs, respectively

Overall, the proposed integrated system exhibits promising potential for marine vessel applications, with certain efficiency and power output considerations to be addressed. The thermodynamic analysis provides valuable insights into the system's behavior, laying the foundation for further optimization and development in the pursuit of more efficient and environmentally friendly marine propulsion solutions.

The research on integrating LPG and SOFC technology for marine vessels, though innovative, faces limitations in the parametric study's narrow scope and reliance on validated models without specific experimental data. Further exploration of operational parameters and a deeper understanding of the human-machine interface are crucial for ensuring the practicality of the proposed system. Looking forward, future research could focus on advanced control strategies and the integration of hybrid energy storage systems, providing enhanced system reliability. Additionally, life cycle assessments and investigations into the adaptability of the proposed system to different vessel types would contribute to refining and broadening its applicability in the maritime industry.

Data Availability

Data is availabile upon the requisition.

Conflicts of Interest

The authors declare that there are no conflicts of interest regarding the publication of this article.

Authors' Contributions

Formal analysis was conducted by D.P.Anh; investigation was conducted by B.R.Ryu; methodology was conducted by J. Jung, S. Lee, and K. Yoon; supervision was conducted by H.K.Kang; writing the original draft was conducted by D.P.Anh and B.R.Ryu; writing, reviewing, and editing were conducted by H.K. Kang. All authors have read and agreed to the published version of the manuscript.

Acknowledgments

This work was supported by the Technology Innovation Program funded by the Ministry of Trade, Industry & Energy (MOTIE, Korea) (project name: development of fuel cell system design and analysis platform technology to hydrogen mobility; project number: RS-2022-00144016), the Korea Institute of Marine Science & Technology Promotion (KIMST) funded by the Ministry of Oceans and Fisheries, Korea (20200520 and 20210559), and the Korea Evaluation Institute of Industrial Technology (KEIT) grant funded by the Korea Government (MOTIE) (RS-2023-00285272).

References

[1] M. Minutillo, A. Perna, P. Di Trolio, S. Di Micco, and E. Jannelli, "Techno-economics of novel refueling stations based on ammonia-to-hydrogen route and SOFC technology," *International Journal of Hydrogen Energy*, vol. 46, no. 16, pp. 10059–10071, 2021.

[2] A. Miola, B. Ciuffo, E. Giovine, and M. Marra, *Regulating air emissions from ships: the state of the art on methodologies, technologies and policy options*, Publications Office of the European Union, 2010.

[3] P. A. Duong, B. R. Ryu, J. Jung, and H. Kang, "Comparative analysis on vapor cloud dispersion between LNG/liquid NH3 leakage on the ship to ship bunkering for establishing safety zones," *Journal of Loss Prevention in the Process Industries*, vol. 85, article 105167, 2023.

[4] A. Windecker and A. Ruder, "Fuel economy, cost, and greenhouse gas results for alternative fuel vehicles in 2011," *Transportation Research Part D Transport and Environment*, vol. 23, pp. 34–40, 2013.

[5] S. Lee, S. Oh, and Y. Choi, "Performance and emission characteristics of an SI engine operated with DME blended LPG fuel," *Fuel*, vol. 88, no. 6, pp. 1009–1015, 2009.

[6] DNV GL-Maritime, "Assessment of selected ternative fuels and technologies," *Imo*, vol. 391, pp. 1–48, 2019.

[7] G. Talib Hashem, M. F. al-Dawody, and I. E. Sarris, "The characteristics of gasoline engines with the use of LPG: an experimental and numerical study," *International Journal of Thermofluids*, vol. 18, article 100316, 2023.

[8] D. Burnes and A. Camou, "Impact of fuel composition on gas turbine engine performance," *Journal of Engineering for Gas Turbines and Power*, vol. 141, no. 10, article 101006, 2019.

[9] P. A. Duong, B. R. Ryu, M. K. Song, D. Nam, and H. Kang, "Thermodynamics analysis of a novel designation of LNG solid oxide fuel cells combined system with CO_2 capture using LNG cold energy," *Journal of Engineering Research*, 2023.

[10] P. A. Duong, B. R. Ryu, H. Lee, and H. Kang, "Thermodynamic analysis of integrated ammonia fuel cells system for maritime application," *Energy Reports*, vol. 10, pp. 1521–1537, 2023.

[11] P. A. Duong, B. R. Ryu, S. S. Kyu, H. Jeon, and H. Kang, "Performance analysis of a fuel cells integrated system utilizing liquified natural gas as fuel for a green shipping target," *International Journal of Naval Architecture and Ocean Engineering*, vol. 15, article 100543, 2023.

[12] P. A. Duong, B. Ryu, J. Jung, and H. Kang, "Thermal evaluation of a novel integrated system based on solid oxide fuel cells and combined heat and power production using ammonia as fuel," *Applied Sciences*, vol. 12, no. 12, p. 6287, 2022.

[13] A. A. Sinha, Sanjay, M. Z. Ansari, A. K. Shukla, and T. Choudhary, "Comprehensive review on integration strategies and numerical modeling of fuel cell hybrid system for power & heat production," *International Journal of Hydrogen Energy*, vol. 48, no. 86, pp. 33669–33704, 2023.

[14] A. A. Sinha, G. Saini, Sanjay et al., "A novel comparison of energy-exergy, and sustainability analysis for biomass-fueled solid oxide fuel cell integrated gas turbine hybrid configuration," *Energy Conversion and Management*, vol. 283, article 116923, 2023.

[15] A. A. Sinha, Sanjay, M. Z. Ansari, A. Kumar Shukla, T. N. Verma, and T. Choudhary, "Thermodynamic assessment of biomass-fueled solid oxide fuel cell integrated gas turbine hybrid configuration," *Sustainable Energy Technologies and Assessments*, vol. 57, article 103242, 2023.

[16] A. A. Sinha, T. Choudhary, M. Z. Ansari, A. K. Shukla, and A. Arabkoohsar, "Waste heat recovery and exergy-based comparison of a conventional and a novel fuel cell integrated gas turbine hybrid configuration," *Sustainable Energy Technologies and Assessments*, vol. 57, article 103256, 2023.

[17] Y. Bessekon, P. Zielke, A. C. Wulff, and A. Hagen, "Simulation of a SOFC/battery powered vehicle," *International Journal of Hydrogen Energy*, vol. 44, no. 3, pp. 1905–1918, 2019.

[18] F. Chen, S. Zha, J. Dong, and M. Liu, "Pre-reforming of propane for low-temperature SOFCs," *Solid State Ionics*, vol. 166, no. 3–4, pp. 269–273, 2004.

[19] K. Ahmed, J. Gamman, and K. Föger, "Demonstration of LPG-fueled solid oxide fuel cell systems," *Solid State Ionics*, vol. 152-153, no. 153, pp. 485–492, 2002.

[20] C. O. Emordi, A. S. Abdulkareem, O. S. Azeez, and S. Afolabi, "Exergy and energy analysis of solid oxide fuel cell fuelled using methanol propane, and butane," *IOP Conference Series: Earth and Environmental Science*, vol. 173, article 012010, 2018.

[21] X. Liu, D. Xie, J. T. S. Irvine, J. Ni, and C. Ni, "An $FeNbO_4$-based oxide anode for a solid oxide fuel cell (SOFC)," *Electrochimica Acta*, vol. 335, article 135692, 2020.

[22] H. Yan, G. Wang, Z. Lu et al., "Techno-economic evaluation and technology roadmap of the MWe-scale SOFC-PEMFC hybrid fuel cell system for clean power generation," *Journal of Cleaner Production*, vol. 255, article 120225, 2020.

[23] E. Antolini, "Direct propane fuel cells," *Fuel*, vol. 315, article 123152, 2022.

[24] P. A Duong, B. R. Ryu, M. K. Song, H. V. Nguyen, D. Nam, and H. Kang, "Safety Assessment of the Ammonia Bunkering Process in the Maritime Sector: A Review," *Energies*, vol. 16, p. 4019, 2023.

[25] DNV GL, *Comparison of alternative marine fuels*, pp. 1–65, DNV GL AS Maritime, 2019.

[26] G. Nikolaou, B. Herzer, M. Arahata, and R. Basaglia, *LPG for marine engines the marine alternative fuel commercial, passenger, offshore boats/ships, recreational crafts and other boats*, World LPG Assoc., 2017.

[27] F. Musharavati and S. Khanmohammadi, "Performance improvement of a heat recovery system combined with fuel cell and thermoelectric generator: 4E analysis," *International Journal of Hydrogen Energy*, vol. 47, no. 62, pp. 26701–26714, 2022.

[28] A. G. Segarra, *Robust control of a solid oxide fuel cell for combined heat and power*, p. 260, 2017.

[29] T. J. Huang, C. Y. Wu, and C. H. Wang, "Fuel processing in direct propane solid oxide fuel cell and carbon dioxide reforming of propane over Ni-YSZ," *Fuel Processing Technology*, vol. 92, no. 8, pp. 1611–1616, 2011.

[30] S. Woo, S. Baek, and K. Lee, "On-board LPG reforming system for an LPG · hydrogen mixed combustion engine," *International Journal of Hydrogen Energy*, vol. 45, no. 21, pp. 12203–12215, 2020.

[31] J. Zhou, Z. Wang, M. Han, Z. Sun, and K. Sun, "Optimization of a 30 kW SOFC combined heat and power system with different cycles and hydrocarbon fuels," *International Journal of Hydrogen Energy*, vol. 47, no. 6, pp. 4109–4119, 2022.

[32] P. A. Duong, B. Ryu, J. Jung, and H. Kang, "Design, modelling, and thermodynamic analysis of a novel marine power system based on methanol solid oxide fuel cells, integrated proton exchange membrane fuel cells, and combined heat and power production," *Sustainability*, vol. 14, no. 19, article 12496, 2022.

[33] N. Chitgar and M. Moghimi, "Design and evaluation of a novel multi-generation system based on SOFC-GT for electricity, fresh water and hydrogen production," *Energy*, vol. 197, article 117162, 2020.

[34] P. A. Duong, H. J. Kim, B. R. Ryu, and H. Kang, "A quantitative risk analysis during truck-to-ship ammonia bunkering," *Sustainability*, vol. 16, p. 2204, 2024.

[35] A. Fuerte, R. X. Valenzuela, M. J. Escudero, and L. Daza, "Ammonia as efficient fuel for SOFC," *Journal of Power Sources*, vol. 192, no. 1, pp. 170–174, 2009.

[36] V. Eveloy, P. Rodgers, and L. Qiu, "Integration of an atmospheric solid oxide fuel cell - gas turbine system with reverse osmosis for distributed seawater desalination in a process facility," *Energy Conversion and Management*, vol. 126, pp. 944–959, 2016.

[37] Y. Liu, J. Han, and H. You, "Performance analysis of a CCHP system based on SOFC/GT/CO_2 cycle and ORC with LNG cold energy utilization," *International Journal of Hydrogen Energy*, vol. 44, no. 56, pp. 29700–29710, 2019.

[38] P. A. Duong, B. Ryu, C. Kim, J. Lee, and H. Kang, "Energy and exergy analysis of an ammonia fuel cell integrated system for marine vessels," *Energies*, vol. 15, no. 9, p. 3331, 2022.

[39] B. Ryu, P. A. Duong, and H. Kang, "Comparative analysis of the thermodynamic performances of solid oxide fuel cell–gas turbine integrated systems for marine vessels using ammonia and hydrogen as fuels," *International Journal of Naval Architecture and Ocean Engineering*, vol. 15, article 100524, 2023.

[40] S. Woo, W. Kim, J. Lee, and K. Lee, "Performance evaluation of the LPG engine applied to catalytic reforming system for producing hydrogen," *Applied Energy*, vol. 312, article 118757, 2022.

[41] F. Gökaliler, B. Selen Çağlayan, Z. İlsen Önsan, and A. Erhan Aksoylu, "Hydrogen production by autothermal reforming of LPG for PEM fuel cell applications," *International Journal of Hydrogen Energy*, vol. 33, no. 4, pp. 1383–1391, 2008.

[42] F. Cipitì, V. Recupero, L. Pino, A. Vita, and M. Laganà, "Experimental analysis of a 2kWe LPG-based fuel processor for polymer electrolyte fuel cells," *Journal of Power Sources*, vol. 157, no. 2, pp. 914–920, 2006.

[43] H. Chen and M. H. Kim, "Thermodynamic analysis and working fluid selection of a novel cogeneration system based on a regenerative organic flash cycle," *Energies*, vol. 15, no. 21, p. 7843, 2022.

[44] P. Giménez-Prades, J. Navarro-Esbrí, C. Arpagaus, A. Fernández-Moreno, and A. Mota-Babiloni, "Novel molecules as working fluids for refrigeration, heat pump and organic Rankine cycle systems," *Renewable and Sustainable Energy Reviews*, vol. 167, article 112549, 2022.

[45] Z. Pan, L. Zhang, Z. Zhang, L. Shang, and S. Chen, "Thermodynamic analysis of KCS/ORC integrated power generation system with LNG cold energy exploitation and CO_2 capture," *Journal of Natural Gas Science and Engineering*, vol. 46, pp. 188–198, 2017.

[46] R. Adland, H. Jia, and J. Lu, "Price dynamics in the market for liquid petroleum gas transport," *Energy Economics*, vol. 30, no. 3, pp. 818–828, 2008.

[47] A. Behzadi, A. Arabkoohsar, and E. Gholamian, "Multi-criteria optimization of a biomass-fired proton exchange membrane fuel cell integrated with organic rankine cycle/thermoelectric generator using different gasification agents," *Energy*, vol. 201, article 117640, 2020.

[48] E. Shayan, V. Zare, and I. Mirzaee, "On the use of different gasification agents in a biomass fueled SOFC by integrated gasifier: a comparative exergo-economic evaluation and optimization," *Energy*, vol. 171, pp. 1126–1138, 2019.

[49] Z. Wang, H. Chen, R. Xia, F. Han, Y. Ji, and W. Cai, "Energy, exergy and economy (3E) investigation of a SOFC-GT-ORC waste heat recovery system for green power ships," *Thermal Science and Engineering Progress*, vol. 32, article 101342, 2022.

[50] S. Das, D. Kashyap, B. J. Bora, P. Kalita, and V. Kulkarni, "Thermo-economic optimization of a biogas-diesel dual fuel engine as remote power generating unit using response surface methodology," *Thermal Science and Engineering Progress*, vol. 24, article 100935, 2021.